



Finite Element Investigation of the Influence of SiC Particle Distribution on Diamond Cutting of SiCp/Al Composites

Shijin Lu¹ · Zengqiang Li^{1,2} · Junjie Zhang^{1,2}  · Jianguo Zhang³ · Xiaohui Wang⁴ · Yongda Yan¹ · Tao Sun¹

Received: 5 June 2020 / Revised: 30 July 2020 / Accepted: 2 September 2020 / Published online: 25 September 2020
© The Author(s) 2020

Abstract

Characteristics of internal microstructures have a strong impact on the properties of particulate reinforced metal composites. In the present work, we perform finite element simulations to elucidate fundamental mechanisms involved in the ultra-precision orthogonal cutting of aluminum-based silicon carbide composites (SiCp/Al), with an emphasis on the influence of particle distribution characteristic. The SiCp/Al composite with a particle volume fraction of 25 vol% and a mean particle size of 10 μm consists of randomly distributed polygon-shaped SiC particles, the elastic deformation and brittle failure of which are described by the brittle cracking model. Simulation results reveal that in addition to metal matrix tearing, cutting-induced particle deformation in terms of dislodging, debonding, and cracking plays an important role in the microscopic deformation and correlated machining force variation and machined surface integrity. It is found that the standard deviation of particle size to the mean value has a strong influence on the machinability of microscopic particle–tool edge interactions and macroscopically observed machining results. The present work provides a guideline for the rational synthesis of particulate-reinforced metal composites with high machinability.

Keywords SiCp/Al composites · Orthogonal cutting · Particle–tool interaction · Particle distribution · FE simulation

1 Introduction

Aluminum-based silicon carbide composites (SiCp/Al) have been widely used in the aerospace, automotive, machinery, and electronics industries for their unique physical and mechanical properties [1–3]. While mechanical machining is normally required to achieve desired shapes with considerable accuracy, recently cutting technique has also been proposed to process SiCp/Al composites for its high geometrical accuracy and high efficiency [4]. However, the

poor synergetic deformation behavior between hard–brittle SiC reinforcement and soft–ductile Al matrix leads to low machinability of SiCp/Al in cutting process. In particular for the ultra-precision diamond cutting with depths of cut (DOCs) comparable to particle sizes, the underlying machining mechanisms of SiCp/Al are complex due to the strong size effect.

The mechanical properties of SiCp/Al strongly rely on the geometrical characteristics of internal microstructures. For instance, the Young's modulus of SiCp/Al composites containing 70 vol% and 30 vol% SiC particles is 230 GPa and 110 GPa, respectively [5]. Accordingly, the machinability of SiCp/Al composites is greatly affected by intrinsic material parameters such as size and volume fraction of SiC particles. Therefore, a thorough understanding of the influences of geometrical parameters of SiC particles on the machining of SiCp/Al is required. Teng et al. performed cutting experiments of micro- and nano-particle-reinforced SiCp/Al composites. They found that nanoparticles are less likely to break and more likely to form continuous chips during cutting processes than microparticles, which are easy to break and tend to form discontinuous chips. Also, a better machined surface quality can be obtained from nanoparticle-reinforced metal

✉ Junjie Zhang
zhjj505@gmail.com

¹ Center for Precision Engineering, Harbin Institute of Technology, Harbin 150001, China
² Technology and Innovation Research Center of Jiangyan Economic Development Zone, Taizhou 225300, China
³ State Key Laboratory of Digital Manufacturing Equipment and Technology, School of Mechanical Science and Engineering, Huazhong University of Science and Technology, Wuhan 430074, China
⁴ School of Mechanical Engineering, University of Jinan, Jinan 250022, China

matrix composites (MMCs) than microparticle-reinforced MMCs [6]. Cheung et al. experimentally investigated the effect of size and volume fraction of SiC reinforcement in ultra-precision machining of Al6061/SiC composites, and reported that a better surface finish can be achieved with thinner reinforcements or smaller volume fraction of reinforcements [7, 8]. Fathipour et al. performed finite element (FE) simulations to investigate the effect of volume fraction of SiC particles on chip formation in SiCp/Al cutting, and indicated that the size of saw-tooth chip decreases with increasing volume fraction of SiC particles [9]. Sandhiya et al. carried out FE simulations to investigate the influences of volume fraction, size, shape, and distribution of SiC particles on particle–tool edge interactions, chip formation, and residual stress pattern in SiCp/Al cutting. They concluded that the shape of SiC particles has a strong influence on chip morphology: while circular particles undergo minimum squeezing and are likely to debonding with matrix, hexagonal particles are likely to break [10].

Although previous studies have provided valuable insights into the cutting process of SiCp/Al composites, they mainly focused on the influence of size and volume fraction of SiC particles, and there is no work reported on the influence of particle distribution characteristics. In particular, the size of SiC particles in real microstructure of SiCp/Al specimen follows a Gaussian distribution. Wang et al. found that the size of SiC particles with Gaussian distribution ranges from 2 to 18 μm with a mean value of 10 μm in SiCp/Al specimen [11]. While the influence of SiC particle size on the cutting of SiCp/Al has been widely demonstrated, the standard deviation of SiC particle size also has a strong influence on the machinability of SiCp/Al due to different particle–tool edge interactions [12]. Furthermore, simplified assumptions on SiC particles, such as setting particles as linear elastomers, arranging particle shape as sphere, assigning uniform particle size

and distribution, etc. [13–16], have been widely adopted in previous FE simulations, which inevitably deteriorate the accuracy of prediction results. For instance, stress pattern built in the vicinity of reinforcements are significantly different for spherical and polygon particles, which may also result in different machining behaviors of the composites.

Therefore, in the present work, we establish a 2D FE model of diamond cutting of SiCp/Al composites with 25 vol% SiC particles. Reinforced SiC particles with arbitrary polygonal shapes are randomly distributed, and SiC particle sizes ranging from 5 to 15 μm follow a Gaussian distribution. Furthermore, SiC particles described by the brittle cracking model are allowed to undergo elastic deformation and brittle failure. The underlying cutting mechanisms of SiCp/Al, in particular particle–tool interactions and their correlations with machining results, are revealed. Furthermore, four standard deviations of SiC particle distribution, while keeping a constant mean value of 10 μm , are considered to investigate the influence SiC particle distribution characteristics on the cutting of SiCp/Al.

2 Methodology

Figure 1a shows the 2D FE model of orthogonal cutting of SiCp/Al composites, which is composed of a SiCp/Al specimen and a diamond tool. The specimen has a dimension of 120 μm in length and 50 μm in height, which is extracted from a large sample with a dimension of 250 μm in length and 250 μm in height, as shown in Fig. 1b. The large sample consists of randomly distributed polygon-shaped SiC particles with a volume fraction of 25 vol%, and the equivalent diameter of SiC particles follows a Gaussian distribution [11]:

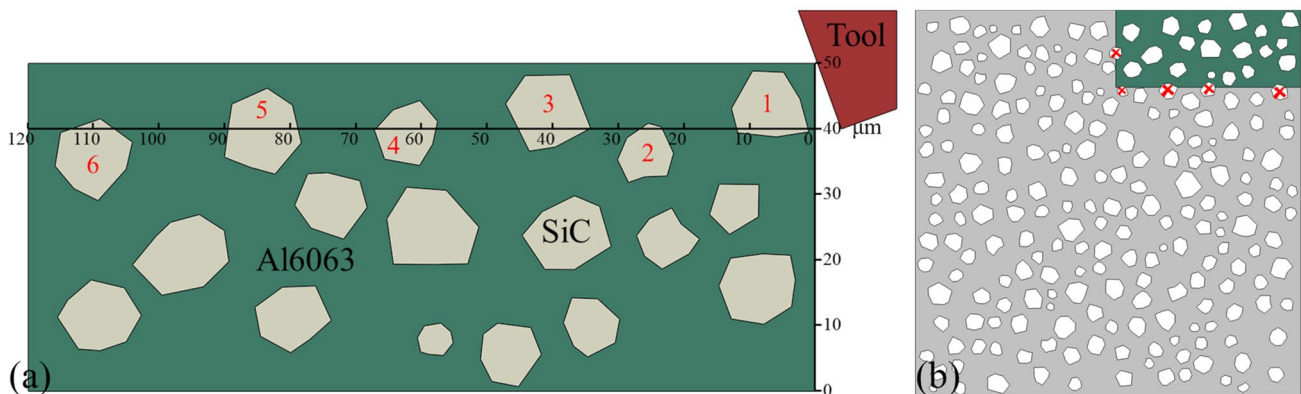


Fig. 1 FE modeling of orthogonal cutting of SiCp/Al composites with a mean value of 10 and a standard deviation of 2. **a** Geometry between tool path and involved particles; **b** large model of SiCp/Al sample

$$p(\bar{d}) = 0.0581 + \frac{40.2915}{\text{Var}} \cdot \exp\left(-0.5 \times \left(\frac{\bar{d} - \text{Ex}}{\text{Var}}\right)^2\right) \quad (1)$$

where Ex is the mean value that is equal to 10 μm, Var is the standard deviation, and *d* is the equivalent diameter of SiC particles. In the present work, four values of Var are considered, as 1, 1.5, 2, and 2.5, respectively. Figure 2a plots the corresponding volume fractions of the equivalent particle diameters for the four standard deviations, which shows that the statistical centralization of particle sizes to the mean value is increased with increasing value of Var. Accordingly, Fig. 2b–e shows microstructure configurations of the SiCp/Al specimen with different standard deviations.

The SiCp/Al specimen is equally meshed by CPE4R element type with an element size of 0.5 μm. Both the left side and the bottom of the specimen are fixed. SiC particles and Al matrix are established as independent parts. While the interfacial bonding between SiC particle and Al matrix is represented by tie constraints, the failure of the Al matrix around SiC particles leads to the debonding of the particle–matrix interface. The simulated diamond tool is treated as a discrete rigid body by ignoring tool wear within the short cutting length of 120 μm. The tool has a rake angle of −20° and a flank angle of 20°. In the FE simulations of

orthogonal cutting process, the diamond tool cuts the specimen surface with a constant DOC of 10 μm and a constant cutting speed of 0.3 m/min.

The elasto-plastic deformation of Al6063 matrix is described by the Johnson–Cook (J–C) model, and a J–C damage criteria based on equivalent plastic strain is employed to achieve material separation and chip formation [17, 18]. The elastic deformation and brittle failure of SiC particles are described by the brittle cracking model implemented in ABAQUS [19], and the detailed model parameters come from Ref. [20]. Table 1 lists the physical properties of the Al6063 matrix and SiC particles used in the FE simulations. Table 2 lists the parameters of the SiC brittle cracking model. The surface-to-surface contact is used to describe

Table 1 Physical parameters of Al6063 and SiC

Material properties	Al6063 [17]	SiC [19]
Thermal conductivity <i>W/(mm K)</i>	193	81
Density (<i>kg/m³</i>)	2.7×10^3	3.13×10^3
Elastic modulus (GPa)	68.9	420
Poisson’s ratio	0.33	0.14
Specific heat capacity <i>J/(kg K)</i>	900	427
Thermal expansion coefficient (<i>K⁻¹</i>)	2.18×10^{-5}	4.9×10^{-6}

Fig. 2 SiCp/Al composites specimen used in this paper. **a** Gaussian curve of the relationship between the equivalent diameter of reinforced SiC particles and corresponding frequency; Microstructure with Var of **b** 1, **c** 1.5, **d** 2 and **e** 2.5

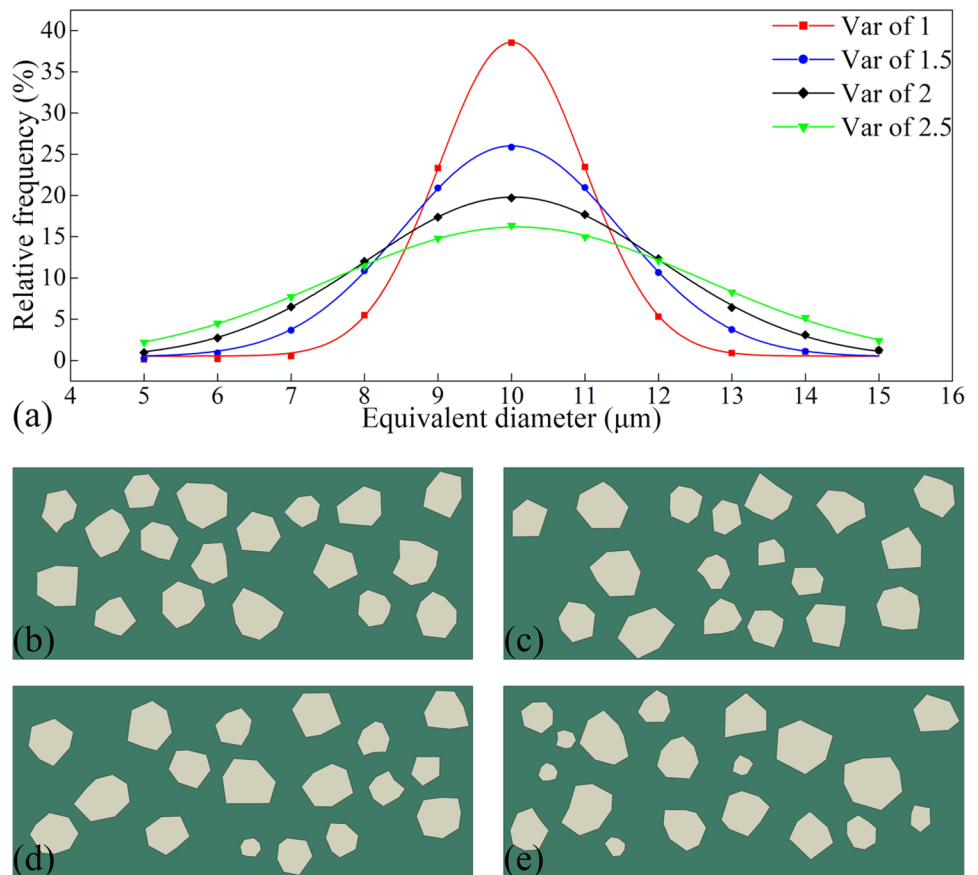


Table 2 Parameters of the brittle cracking model for SiC particles [20]

σ_0 (MPa)	G_f^I (J/m ²)	p	$\epsilon_{\max}^{\text{ck}}$
1500	30	1	0.001

the interaction between tool and Al matrix, as well as the interaction between the tool and SiC particles. Specifically, the first surface is selected as the external surface of the cutting tool, and the second surface is selected as the node type, which includes all nodes of SiC particles and Al matrix. The friction coefficient between the tool and SiCp/Al during machining is 0.45. It should be noted that the consideration of the interaction of removed SiC particles with Al matrix may provide a more accurate description of the cutting force, chip formation, and stress distribution. Since current work mainly focuses on the influence of SiC particle–tool interactions on the cutting process with a relatively small DOC, removed SiC particle–Al matrix interaction after material failure is not considered for simplifying the FE model.

3 Results and Discussion

3.1 Cutting Mechanisms of SiCp/Al Composites

FE simulation of orthogonal cutting of SiCp/Al composites with a Var of 2 is performed to elucidate the involved cutting mechanisms. Figure 1a shows that there are six SiC particles interacting with the tool path within a cutting distance of 120 μm . According to the relative positions of cutting tool edge with respect to the center of mass (COM) of involved

SiC particles, the particle–tool edge interactions can be categorized into three scenarios: the tool edge is above particles 2 and 6 (herein referred to as Upper), the tool edge traverses particles 4 and 5 (herein referred to as Middle), and tool edge is below particles 1 and 3 (herein referred to as Lower). It should be noted that the influence of SiC particle–tool interaction on cutting results is notably for either small or large cutting depth. Dabade et al. indicated that particle fracture and plowing also exist in SiCp/Al cutting with a large DOC of 1 mm [21]. Since the equivalent diameter of SiC particles follows a Gaussian distribution and SiC particles are randomly distributed in an Al matrix, the current FE model is also capable of addressing the influence of the relative position between the tool and particles.

Figure 3 plots variations of cutting force and thrust force with cutting length in the FE simulation of cutting process of SiCp/Al composites with a Var of 2. Moreover, each cutting period in the vicinity of individual SiC particles is highlighted by a green rectangular frame. Figure 3 shows that both the cutting force and thrust force increase with the approaching tool edge towards the particle, and reach local maximum values when cutting is performed on the particle, followed by a decrease due to moving away from the particle. Moreover, the significant fluctuations in both cutting force and thrust force originate from deformation of both Al matrix and SiC particles.

Figure 3 also suggests that SiC particle–tool edge interactions have a strong influence on the evolution of machining force. For particles 1 and 3, which are both above the tool edge, the local maximum value of cutting force for particle 3 is significantly higher than that for particle 1.

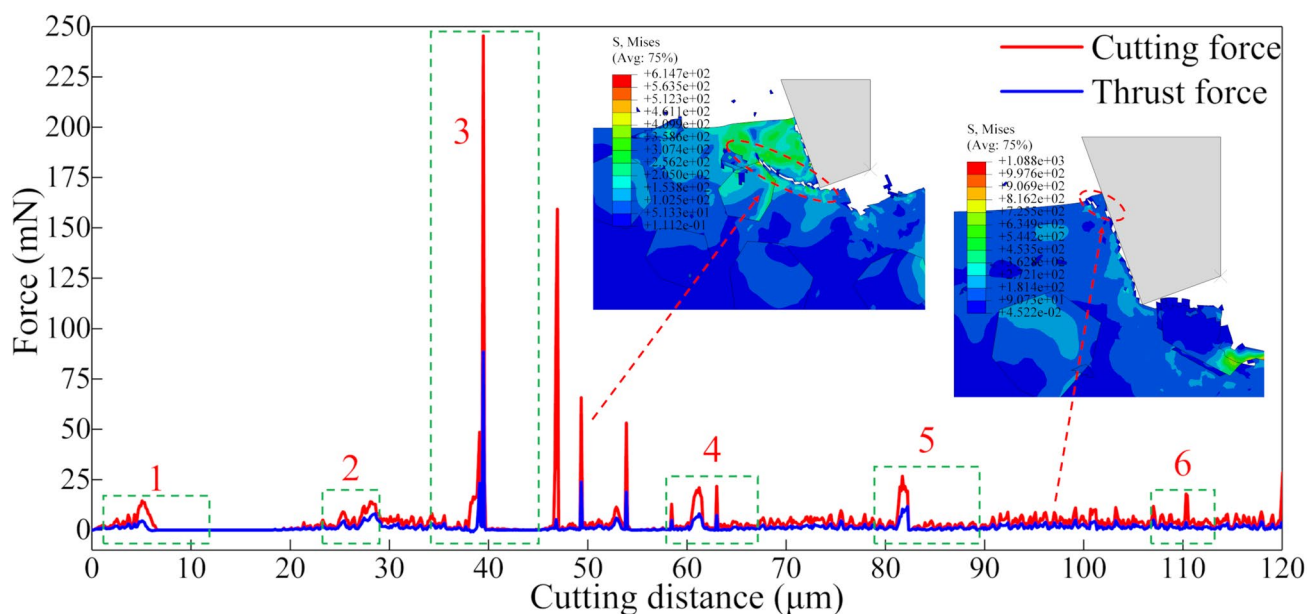


Fig. 3 Variations of cutting force and thrust force with cutting distance in FE simulation of cutting process of SiCp/Al with a Var of 2

The discrepancy in machining force variation between particles 1 and 3 can be attributed to different deformation behaviors: while particle 1 is completely removed with formed chips, particle 3 undergoes a serious fracture. While particles 4 and 5 are both traversed by the tool edge, the characteristics of cutting force variation are similar. Although particles 2 and 6 are both below the tool edge, the fluctuation of cutting force for particle 2 is more pronounced than that for particle 6. While the machining force variation for matrix cutting between particles 1 and 2 is smooth, there are strong fluctuations in cutting force for the rest inter-particle cutting. In particular, there is a significant increase of cutting force for the Al matrix cutting between particles 3 and 4, which is attributed to the bulk removal of Al matrix. When the Al matrix between particles 5 and 6 removes in the form of debris, only a slight vibration of cutting occurs. In order to verify whether the FE model adopted is sufficient to reflect the cutting force evolution and surface defect characteristics during the cutting process, a large model with a cutting distance of 250 μm is also extracted from Fig. 1b. The other parameters are the same for each model. The derived average cutting force and surface roughness from the model with a cutting distance of 250 μm is 4.234 mN and 1.45 μm , respectively. Correspondingly, the error of average cutting force and surface roughness between the cutting distances of 120 μm and 250 μm is 4.213% and 6.618%, respectively. Thus, the model with a small cutting length of 120 μm is sufficient to describe cutting force evolution and surface defect characteristics during the cutting process of SiCp/Al.

Figure 4a, b respectively plots the localized variation of cutting force and thrust force in the vicinity of particles 2 and 3 in the FE simulation of cutting process of SiCp/Al composite with a Var of 2, and for each particle, four representative points are highlighted by sequential numbers. Furthermore, Fig. 4c, e, g, i and Fig. 4d, f, h, j present cutting configurations of particle 2 and particle 3 at different cutting distances, indicated by numbers shown in Fig. 4a, b, respectively.

Figure 4c shows that when the tool edge is approaching particle 2, the Al matrix on the right side of particle 2 is subjected to tensile stress. With the advancement of the tool edge, Fig. 4e indicates that there is tensile stress and compressive stress concentrated in the upper and lower parts of particle 2, respectively, which subsequently leads to the rotation of particle 2. Further cutting action leads to the failure of Al matrix under tensile stress, which in turn results in the debonding of particle 2 from the surrounding Al matrix, as shown in Fig. 4g. Figure 4i shows that since particle 2 is partially broken, the particle–tool edge interactions disappear. Figure 4 shows that the cutting force for particle 2 reaches its local maximum value before particle broken, after which the cutting force is reduced accompanied with chip formation.

Figure 4d shows instantaneous maximal principal stress contours of the local specimen after particle 3 is moved forward by a distance of 0.2 μm . While there is a high concentration of compressive stress in the contact region between tool edge and particle 3, the Al matrix below particle 3 is subjected to high tensile stress, which indicates that particle 3 has a high tendency to be pulled out. Consequently, the unprocessed surface of SiCp/Al specimen is curved compared to the pristine surface, as shown in Fig. 4f. Since the tensile stress value in the bottom of particle 3 is the first to reach the maximum tensile stress limit of SiC, Fig. 4h demonstrates that the broken of particle 3 firstly occurs in the opposite end of the SiC particle–tool edge contact. Finally, particle 3 is completely broken, which is caused by the cutting action, as shown in Fig. 4j. Correspondingly, the cutting force for particle 3 continuously increases to its local maximum value. In this study, the dispersion of SiC particles into the Al matrix accounts for the discrete chip in the cutting process shown in Fig. 4i, j. Furthermore, the used cutting tool has a negative rake angle, which is not beneficial for continuous chip formation due to compressive stress.

Figure 5a presents the simulated configuration of SiCp/Al specimen with a Var of 2 colored by instantaneous maximal principal stress after cutting. In order to clearly show the evolution of SiC particles before and after the cutting process, positions of the original particles are also presented with red lines. It is intuitively observed from Fig. 5a that there are different failure modes of SiC particles occurring: complete removal within formed chip composed of Al matrix (particles 1 and 3); debonding from Al matrix (particles 4 and 5); crushed particles remaining in Al matrix after being partially broken (particles 2 and 6). The observed different deformation modes of SiC particles are closely associated with different particle–tool edge interactions based on the geometrical orientations. Moreover, it is found from Fig. 5a that tensile stress exists only in subsurfaces with a depth of 5 μm , while compression stress appears in areas with greater depths. Figure 5b further plots the profile of machined surfaces in terms of surface height, which indicates that subsurface damage is dominated by particle–matrix debonding (particle 2). Furthermore, the rebound of particle 5 leads to a surface pile up with a height of 4.5 μm formed on the machined surface.

3.2 Influence of SiC Particle Distributions

To address the influence of SiC particle distributions on the diamond cutting of SiCp/Al composites, FE simulations are performed to investigate the cutting processes of SiCp/Al with the other three standard deviations Vars of 1, 1.5, and 2.5, in addition to the Var of 2. The other configuration parameters as well as cutting conditions are the same for each standard deviation Var.

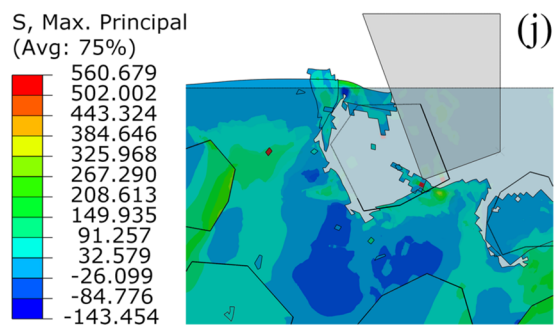
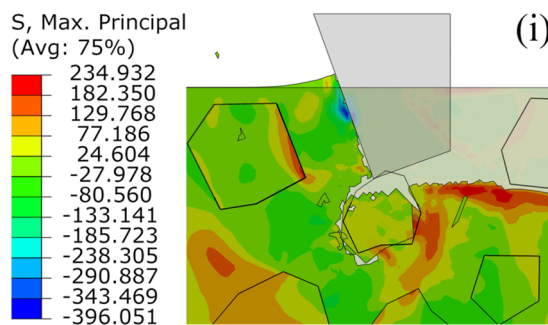
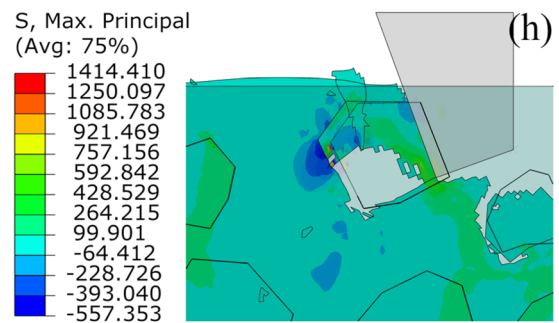
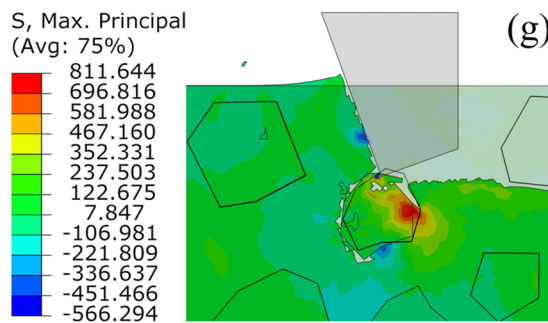
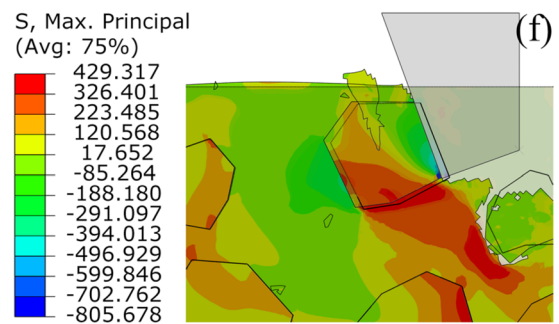
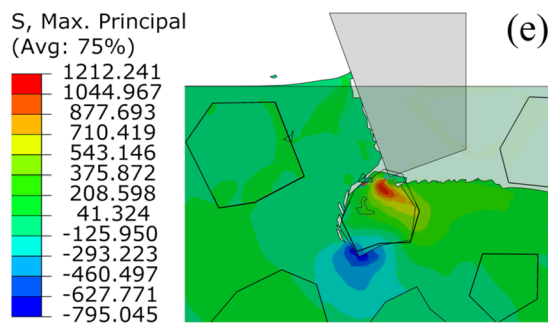
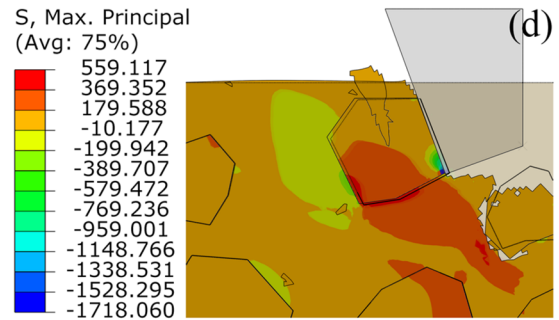
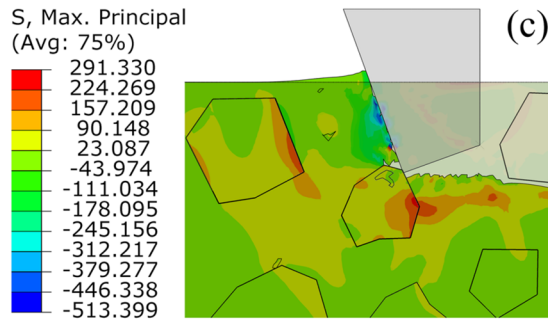
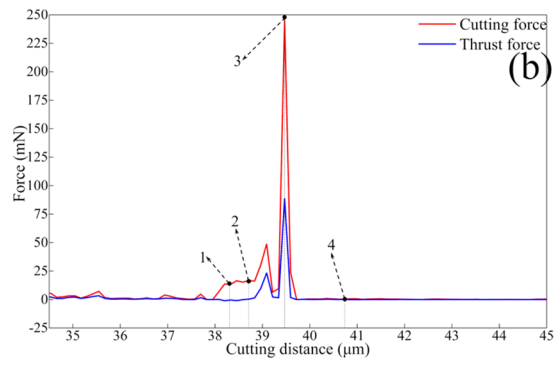
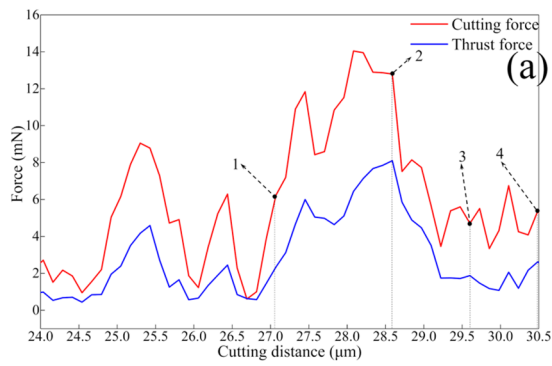


Fig. 4 FE simulation results of particle–tool interactions in orthogonal cutting of SiCp/Al composites with a Var of 2. Localized variation of cutting force for cutting of **a** particle 2 and **b** particle 3. Cutting configuration of particle 2 at a cutting distance of **c** 27.1 μm , **e** 28.6 μm , **g** 29.6 μm , and **i** 30.5 μm ; cutting configuration of particle 3 at a cutting length distance of **d** 38.35 μm , **f** 38.75 μm , **h** 39.5 μm , and **j** 40.8 μm

Figure 6a, b plots variations of cutting force and thrust force for the four Vars, respectively, which indicate a maximum cutting force and thrust force with the Var of 1.5. In addition, since the number of involved SiC particles on the tool path is the largest for the Var of 1.5, it can be seen that the number of peaks of both cutting force and thrust force is also the largest. The number of cutting force peaks is the lowest for the Var of 1. Figure 6c plots variations of average cutting force and thrust force with Var. The average cutting force or thrust force for Vars of 1 and 2 are essentially the same, and their values are smaller than those for the other two Vars. Both cutting force and thrust force are maximum for the Var of 1.5.

Figure 7 presents simulated configurations of SiCp/Al specimen with four different Vars after cutting, which indicates that the maximum compressive stress for the Var of 2.5 is significantly higher than that for the other three Vars. The compressive stress is mainly distributed in the Al matrix between adjacent SiC particles, and the connected particles also have a partial compressive stress distribution region. The deformation modes of SiC particles mentioned in the previous section, such as dislodge, fracture, and dislocation, are also reflected in the cutting results with different value of Vars. Figure 7d shows that the machined surfaces of the first and last particles on the cutting path have similar flatnesses to the machined surface of the

surrounding Al matrix for the Var of 2.5, which is conducive to improve machined surface quality of the specimen.

Figure 8a plots the profile of machined surface for the four Vars. While protrusion of the machined surface only occurs for the Var of 2, the Vars of 1.5 and 2.5 have the cavity with the largest depth of 9 μm . The Var of 1 has the maximum width of cavity of 30 μm . Figure 8b further plots variations of simulated surface roughness for the four Vars. The surface roughness has a maximum value for the Var of 1.5 and a minimum value for the Var of 2. The evolution of surface roughness has the same trend with the average cutting force. Therefore, with the comprehensive consideration of the number of pits and roughness values of the machined surface, the large range of SiC particle size distribution is beneficial to achieve high machined surface quality.

4 Conclusions

In summary, we investigate the machinability of SiCp/Al composites in ultra-precision diamond cutting by 2D FE modeling and simulation. The simulated SiCp/Al composite consists of randomly distributed polygon-shaped SiC particles, and the elastic deformation and brittle failure of SiC particles are described by the brittle cracking model. FE simulation results reveal that the SiC particle–tool edge interactions have a strong dependence on the geometry between the tool edge and particle position, and also have a close correlation with machined surface integrity. Specifically, while tool–particle interaction occurring in the lower middle part of particles leads to a smooth machined surface due to complete removal of SiC particles within the formed chip, crushed particles remaining in the Al matrix induced by particle–tool edge interaction occurring in the upper

Fig. 5 FE simulation of machined surface morphology after cutting of SiCp/Al composites with a Var of 2. **a** Configuration of machined surface. **b** Profile of machined surface

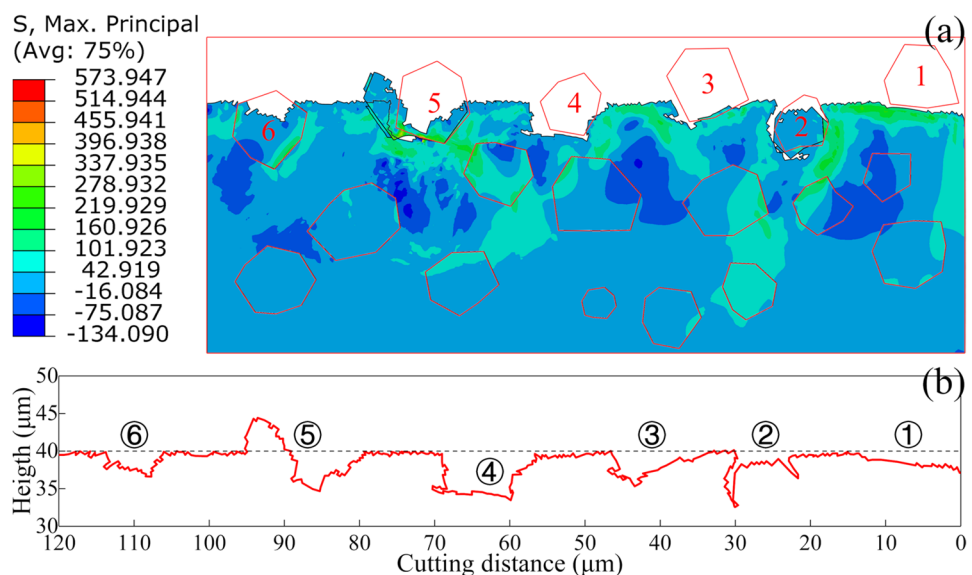


Fig. 6 Variation of machining force in FE simulations of SiCp/Al composites with different SiC particle distributions. **a** Variation of cutting force; **b** variation of thrust force; **c** variation of average cutting force and thrust force with standard derivation of SiC particle size

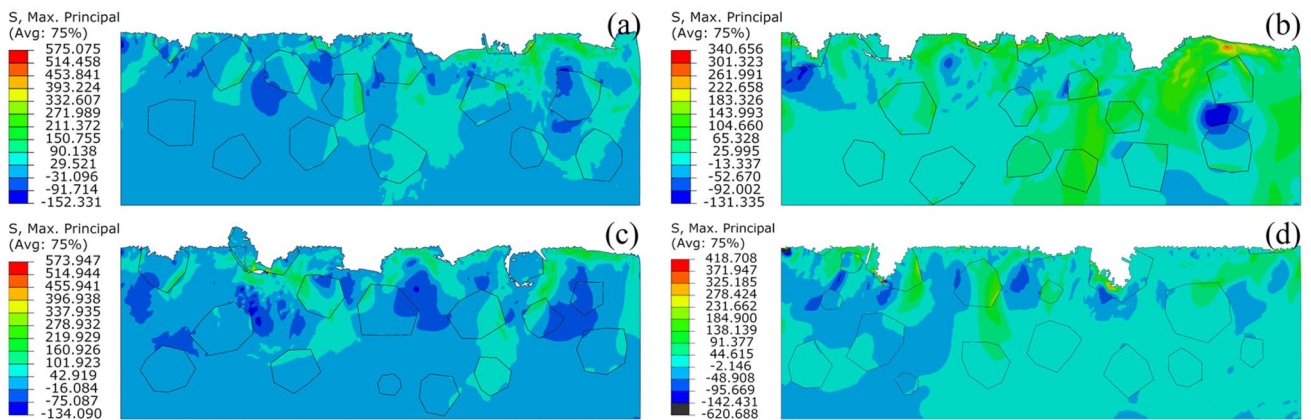
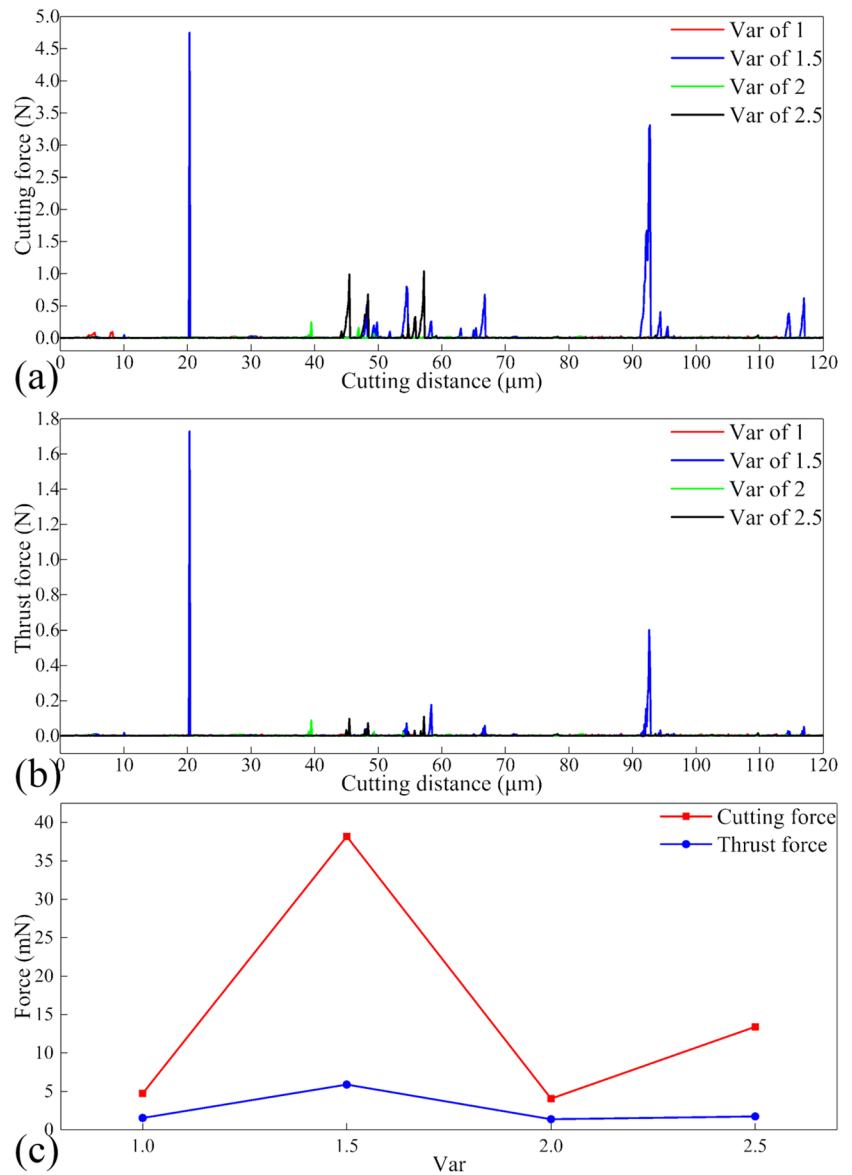


Fig. 7 Simulated machined surface of SiCp/Al composites with different Vars. Configuration of specimen for the Var of **a** 1; **b** 1.5; **c** 2.0; **d** 2.5

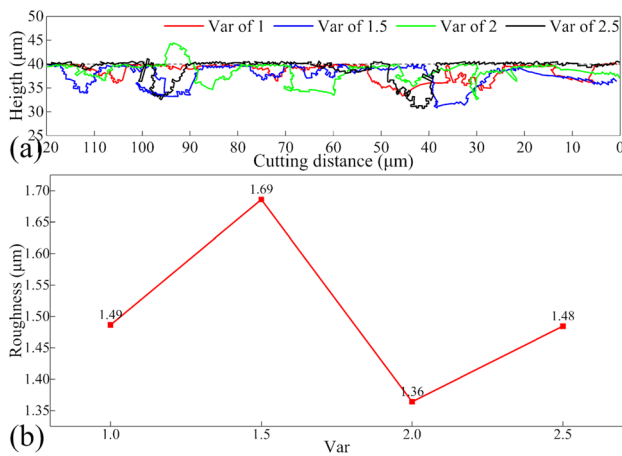


Fig. 8 Characterization of machined surface quality in FE simulations of SiCp/Al composites with different SiC particle distributions. **a** Profiles of machined surface for the four Vars; **b** Variations of surface roughness for the four Vars

middle part of the particles also benefits surface integrity, but debonding of SiC particles from Al matrix induced by tool–particle interaction occurring in the middle part of particles significantly deteriorates surface integrity due to cavity formation. Furthermore, SiC particle–tool edge interactions also have a great impact on machining force variations and residual stress distribution. FE simulations of the influence of SiC particle distribution demonstrate that it is easier to obtain a better machining surface quality of SiCp/Al in cutting processes with a larger size distribution range.

Acknowledgements Funding was provided by National Natural Science Foundation of China (Grant No. 51761135106), Fundamental Research Funds for the Central Universities, Science Challenge Project (Grant Nos. TZ2018006-0201-02, TZ2018006-0205-02) and State Key Lab of Digital Manufacturing Equipment and Technology (Grant Nos. DMETKF 2018007, DMETKF2019016).

Open Access This article is licensed under a Creative Commons Attribution 4.0 International License, which permits use, sharing, adaptation, distribution and reproduction in any medium or format, as long as you give appropriate credit to the original author(s) and the source, provide a link to the Creative Commons licence, and indicate if changes were made. The images or other third party material in this article are included in the article's Creative Commons licence, unless indicated otherwise in a credit line to the material. If material is not included in the article's Creative Commons licence and your intended use is not permitted by statutory regulation or exceeds the permitted use, you will need to obtain permission directly from the copyright holder. To view a copy of this licence, visit <http://creativecommons.org/licenses/by/4.0/>.

References

- Lee RS, Chen GA, Hwang BH (1995) Thermal and grinding induced residual stresses in a silicon carbide particle-reinforced aluminium metal matrix composite. *Composites* 26(6):425–429

- Dandekar CR, Shin YC (2012) Modeling of machining of composite materials: a review. *Int J Mach Tools Manuf* 57:102–121
- Li P, Ji XH, Xue KM (2018) Correlation between the thermal responses and microstructure patterns in aluminum-based silicon carbide composites (SiCp/Al) consolidated by different high pressure torsion schemes. *Mater Sci Eng Technol* 49(9):1117–1124
- Bai YC, Shi ZQ, Lee YJ, Wang H (2020) Optical surface generation on additively manufactured AlSiMg0.75 alloys with ultrasonic vibration-assisted machining. *J Mater Process Technol* 280:116597
- <http://www.matweb.com>
- Teng XY, Chen WQ, Huo DH, Shyha I, Lin C (2018) Comparison of cutting mechanism when machining micro and nanoparticles reinforced SiC/Al metal matrix composites. *Compos Struct* 203:636–647
- Cheung CF, Chan KC, To S, Lee WB (2002) Effect of reinforcement in ultra-precision machining of Al6061/SiC metal matrix composites. *Scr Mater* 47(2):77–82
- Cheung CF, Lee WB (2000) A theoretical and experimental investigation of surface roughness formation in ultra-precision diamond turning. *Int J Mach Tools Manuf* 40(7):979–1002
- Fathipour M, Zoghipour P, Tarighi J, Yousef R (2012) Investigation of reinforced SiC particles percentage on machining force of metal matrix composite. *Mod Appl Sci* 6(8):9–20
- Nithiya Sandhiya YJ, Thamizharasan MM, Ajay Subramanyam BV, Vijay Sekar KS, Suresh Kumar S (2018) Finite element analysis of tool particle interaction, particle volume fraction, size, and distribution in machining of A356/SiCp. *Mater Today Proc* 5(8):16800–16806
- Wang T (2015) Basic research on high volume milling of high volume fraction SiCp/Al composite. Beijing Institute of Technology, Beijing
- Lu SJ, Zhang JJ, Li ZQ, Zhang JG, Wang XH, Hartmaier A, Xu JF, Yan YD, Sun T (2020) Cutting path-dependent machinability of SiCp/Al composite under multi-step ultra-precision diamond cutting. *Chin J Aeronaut* (in press)
- Shao JC, Xiao BL, Wang QZ, Ma ZY, Yang K (2011) An enhanced FEM model for particle size dependent flow strengthening and interface damage in particle reinforced metal matrix composites. *Compos Sci Technol* 71(1):39–45
- Pramanik A, Zhang LC, Arsecularatne JA (2007) An FEM investigation into the behavior of metal matrix composites: tool–particle interaction during orthogonal cutting. *Int J Mach Tools Manuf* 47(10):1497–1506
- Fathipour M, Hamedi M, Yousefi R (2013) Numerical and experimental analysis of machining of Al (20 vol% SiC) composite by the use of ABAQUS software. *Mater Sci Eng Technol* 44(1):14–20
- Umer U, Ashfaq M, Qudeiri JA, Hussein HMA, Danish SN, Al-Ahmari AR (2015) Modeling machining of particle-reinforced aluminum-based metal matrix composites using cohesive zone elements. *Int J Adv Manuf Technol* 78(5–8):1171–1179
- Chen XL, Wang XB, Xie LJ, Wang T, Ma B (2018) Determining Al6063 constitutive model for cutting simulation by inverse identification method. *Int J Adv Manuf Technol* 98(1–4):47–54
- Mabrouki T, Girardin F, Asad M, Rigal J (2008) Numerical and experimental study of dry cutting for an aeronautic aluminium alloy (A2024-T351). *Int J Mach Tools Manuf* 48(11):1187–1197
- Hibbitt, Karlsson, Sorensen (2001) ABAQUS/Explicit: user's manual. Hibbitt, Karlsson and Sorensen Incorporated
- Wang YF, Liao WH, Yang K, Chen WQ, Liu TT (2018) Investigation on cutting mechanism of SiCp/Al composites in precision turning. *Int J Adv Manuf Technol* 100(1–4):963–972
- Dabade UA, Joshi SS, Balasubramaniam R, Bhanuprasad VV (2007) Surface finish and integrity of machined surfaces on Al/SiCp composites. *J Mater Process Technol* 192:166–174